

CHARACTERIZATION OF SAR IMAGES IN THE 2010 HAITI EARTHQUAKE

Pralhad Uprety¹⁾ and Fumio Yamazaki²⁾

1) Professor, Dept. of Urban environment System, Chiba University, Japan

2) PhD Student, Dept. of Urban environment System, Chiba University, Japan

pralhaduprety@yahoo.com, yamazaki@tu.chiba-u.ac.jp

Abstract: Radar remote sensing has advantages over the optical remote sensing since it is not affected by the cloud cover as well as its capability of operation during both day and night. With the advancement of high resolution radar remote sensing, fine details of subject under consideration can be achieved. On 12th Jan 2010, earthquake of moment magnitude 7 hit Haiti causing widespread casualty and destruction to the infrastructures. This earthquake was responsible for death of 217,000 people, injury to 300,000 people and homeless for 1.2 million people. It was the deadliest event in the history of Haiti. Two sets of high resolution radar imageries from TerraSAR-X (each set of pre-event and post-event imagery) were used for the damage detection in city center of Port-au-Prince, the capital of Haiti. Radar characteristics like correlation coefficient and backscatter differences were calculated and threshold values of them were overlaid to optical images. Changes like building damage after the earthquake were clearly recognized.

1. INTRODUCTION

Disasters have been defined as a serious disruption of a community or a society causing widespread human, material, economic and environmental losses which exceed the ability of the community or society to cope using its own level of the resources (ISDR 2010).

As SAR images are cloud and time independent (both day and night operation) data source, they are very reliable source of data acquisition particularly in the times of the emergency. High resolution imagery as from TerraSAR-X has opened a new dimension in delivering the needs of the emergency and post-disaster situation monitoring. These characteristics are the primary reasons leading to the utilization of SAR in the disaster situations including earthquakes, wildfire and so on (Matsuoka and Yamazaki 2004, 2010; Stramondo et al. 2006; Thao et al. 2010). In this paper, we analyze the damaged buildings of the Port-au-Prince city center in Haiti using high-resolution TerraSAR-X images.

2. THE HAITI EARTHQUAKE

Haiti in general and Port-au-Prince in particular had very little experience of earthquakes in the past. Notable past earthquakes include that of earthquakes 1701, 1751, 1770 and 1860 (Eberhand et al. 2010). After about 150 years of gap a large earthquake of moment magnitude 7.0 hit Haiti on January 12th, 2010. The epicenter was at Leogane (Lat 18.44°N, Long 72.57°W) about 17 km from capital city

Port-au-Prince. The depth of earthquake was 13 kilometer. Mostly cities like Leogane, Jacmel, Petit-Goave and Port-au-Prince were affected. The earthquake caused 217,000 fatalities; over 300,000 injuries and more than a million of displaced people resulting in the deadliest event caused by natural disasters in the history of Haiti. Many important structures including presidential palace, legislative palace, national cathedral, and headquarter of United Nations, police stations, hospitals, schools, sea port and university were severely damaged. 403,176 buildings were damaged (UNDP 2010). Economic loss is USD 7.9 billion, which is just over 120 percent of the country's gross domestic product in 2009 (Government of Haiti 2010). The burden of the earthquake is such that even after the 2 years of the event half a million people are living in the tents (Reliefweb 2012) and only 5 % of the rubble (out of 19 million cubic meters) could be removed from the street (Time 2010).

2.1 The 2010 Haiti earthquake and SAR data

SAR data employed in this research is from the TerraSAR-X satellite system (X-band, $\lambda=31$ mm and $f = 9.6$ GHz). Pre-event SAR data was from September 17, 2008 (about 15 months before the event) and post-event data was from January 14, 2010 (2 days after the event) as shown in Figure 1. Acquisition mode of these data is stripmap with polarization HH (single). Incidence angle is 39.32 degree. The path of satellite was ascending with right hand look. These images have pixel resolution of 1.25 meter. The employed data was standard product (2A) and it was

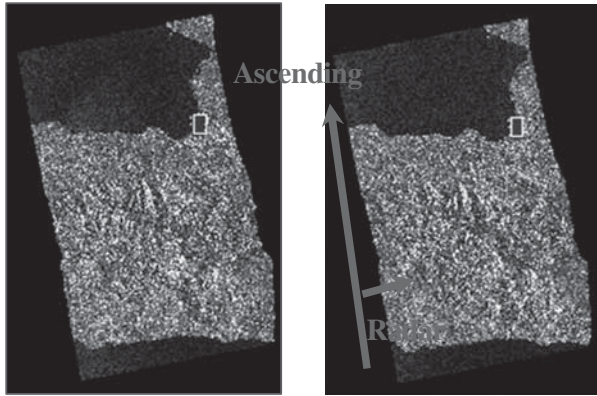


Figure 1 SAR data with blue rectangle showing the area of interest

radiometrically corrected, sensor corrected, geometrically corrected and mapped to a cartographic projection by the data provider.

Besides the SAR data, we also use the optical satellite images. The Pre-event image was from QuickBird, QB, (Feb 4, 2009). Similarly, post-event images were from GeoEye (Jan 13, 2010), WorldView-2 (Jan 15, 2010) and images from Google Earth.

2.2 Damage detection methodology

The study area was chosen in such a way that it encompasses the downtown of capital city, covering the most visible damage like presidential palace and an area both common in an optical and radar imageries. After selecting the study area accurate positioning of the two SAR images was done. These images were re-sampled changing the pixel size from 1.25 m to 0.6 m so that it can be compared to high resolution pan-sharpened optical images. Lee adaptive filter (Lee 1980) with a 21×21 pixel window was applied to each image for speckle removal in the SAR images.

Radiometric calibration of each intensity image was done utilizing the equations (1), (2), and (3) (Breit et al. 2010; Infoterra 2008). The backscattering coefficients obtained from the pre- and post-event SAR images have been used for change/damage detection (Yonezawa and Takeuchi 2001, Matsuoka and Yamazaki 2005, 2007). We also calculate backscatter characteristics like backscattering difference value (d) and correlation coefficient (r) within a 21×21 pixel window of the pre- and post-event image using equations (1) and (2). Figure 2 shows the calibrated images of the study area.

$$d = \bar{I}a_i - \bar{I}b_i \quad (1)$$

$$r = \frac{N \sum_{i=1}^N I a_i I b_i - \sum_{i=1}^N I a_i \sum_{i=1}^N I b_i}{\sqrt{\left(N \sum_{i=1}^N I a_i^2 - \left(\sum_{i=1}^N I a_i \right)^2 \right) \left(N \sum_{i=1}^N I b_i^2 - \left(\sum_{i=1}^N I b_i \right)^2 \right)}} \quad (2)$$

Here, $I a_i$, $I b_i$ represent the i -th pixel values of the post-event

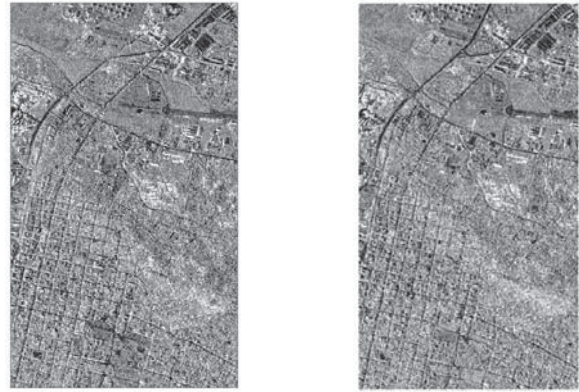


Figure 2 Calibrated images of the study area

and pre-event images respectively and $\bar{I}a_i$, $\bar{I}b_i$ are the average values of 21×21 pixels surrounding the i -th pixel.

Finally, threshold values of correlation coefficient (r) and backscattering difference (d) were selected by trial and error method to detect the damage distribution. The threshold values used are $r \leq 0.25$ as low correlation and $d \leq -4$ dB & $d \geq 4$ dB as the high backscatter difference. The Normalized Density Vegetation Index (NDVI) was calculated from the pre-event QuickBird image. Low NDVI (≤ 0.1) was utilized for removing the vegetation in the study area. The accuracy of damage detection by SAR was evaluated by overlying the results in sample areas in low-, moderate- and high- density areas against the satellite optical images. For the low- and moderate- density areas, damages to buildings (Grades 3, 4 and 5) were transferred from the post-disaster need assessment (PDNA) survey atlas to the GIS environment. PDNA atlas was prepared by UNITAR/UNOSAT in collaboration with different agencies including the World Bank (UNITAR et al. 2010). Building polygons of the sampled areas were drawn over the satellite images. Threshold values from the NDVI, r and d were overlaid on the building footprint and ratio was taken to determine the percentage of area covered by the combined area of the backscatter characteristics. Figure 3 shows result of percentage of overlaid areas of threshold backscatter characteristics upon the building footprints of different damage grades based on EMS scale. Grade 3, Grade 4 and Grade 5 are damaged buildings while Grade 1 and Grade 2 represent undamaged buildings. Based on the Figure 3, threshold value of 27% was taken for the damage detection. If the combined area of the overlapped backscatter characteristics is equal or less than 27% of building footprint then it will be undamaged otherwise damaged. For this purpose we divide buildings into 2 groups namely damaged buildings (Grades 3, 4, and 5) and undamaged buildings (Grade 1 and 2). Regarding the high density area, area based damage estimation was carried out. For this purpose, we calculate the areas of sampled block and combined area of the overlapped threshold values from NDVI, r and d .

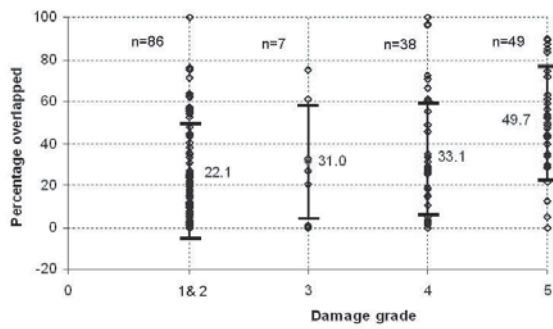


Figure 3 Graph showing the percentage of overlaid areas of threshold NDVI and backscatter characteristics to the building footprints of different damage grades. Error bar is drawn for each mean value with 1 standard deviation. n is the number of buildings in each grade

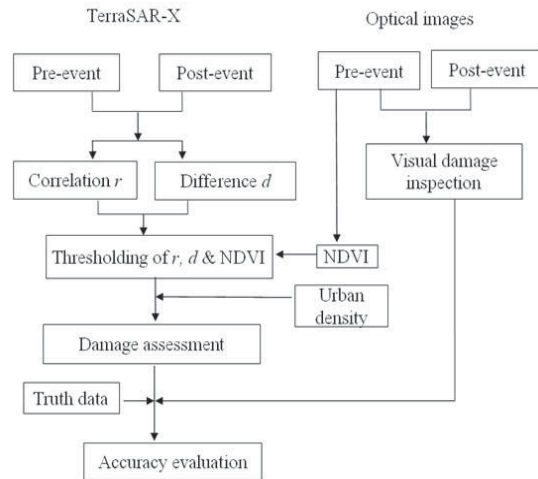


Figure 4 Flow chart of methodology adopted in this study

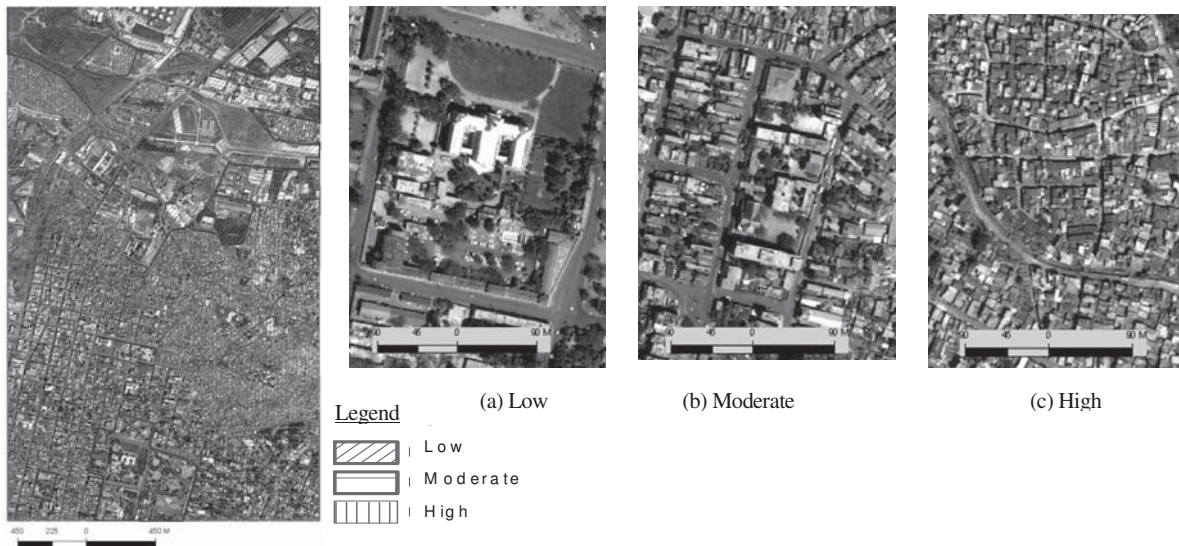


Figure 5 Classification of study area based upon urban density. Example of each class is given (a) low- (b) moderate-(c) high-density area

Percentage of the probable damage areas was then calculated. Figure 4 shows the flowchart of methodology adopted in the study.

3. RESULTS AND DISCUSSION

Figure 5 shows the classification of the study area based upon urban density. Example of each class is given in the inset.

Figure 6 shows the result of urban classification and the corresponding color composite, correlation and backscattering map. Figure 6(a) shows the urban density and the sampled areas of each density class while Figure 6(b) is the composite of calibrated SAR images (red: post-event, cyan: pre-event). Red color marks the possible changes in aftermath of the earthquake; cyan areas represent decreased

backscatter while grey areas are the unchanged areas over the time. Likewise, Figure 6(c) and Figure 6(d) are the correlation and backscattering difference images respectively. Correlation value ranges from -0.9 to 1 while backscattering coefficient difference ranges from -28.1 to 28.2 dB.

When we overlay the union of threshold $NDVI(\leq 0.1)$ and backscatter characteristics ($r \leq 0.25$ and $d \leq -4$ dB & $d \geq 4$ dB) in low density area as in presidential palace (Figure 7), it was found that out of 16 damaged building footprints (Grade 3, Grade 4 and Grade 5), 12 building footprints had the threshold areas of more than 27%. As discussed in methodology they represent the damaged buildings. Similarly, 7 out of 10 non-damaged could be correctly identified. It is to be noted that non-damaged buildings were also identified as damaged buildings. Radar backscatter is affected by the path of satellite, building layout and even

vegetation. When the orientation of tall building is towards the radar path, then the adjacent short buildings are affected by it. This may happen to the main building in the presidential complex and undamaged building was identified as damaged one.

Similarly, if we overlay the union of threshold values of NDVI (≤ 0.1), low correlation ($r \leq 0.25$) and high backscatter difference ($d \leq -4$ dB & $d \geq 4$ dB) in moderate density area as in Figure 8 we noticed that out of 6 damaged buildings 4 buildings could be correctly identified by our threshold value (overlay percentage of union of threshold

values within the building footprints $\leq 27\%$ as undamaged and more than the threshold as damaged). Out of 16 undamaged buildings 10 could be correctly recognized. Table 1 shows the error matrix of the low- and moderate-density areas. Out of 78 damaged buildings, 50 buildings could be correctly identified while out of the 86 undamaged buildings 60 buildings were correctly identified. The producer's accuracy for the damaged buildings was 64.1% while user's accuracy was 65.8%. Overall accuracy is 67%.

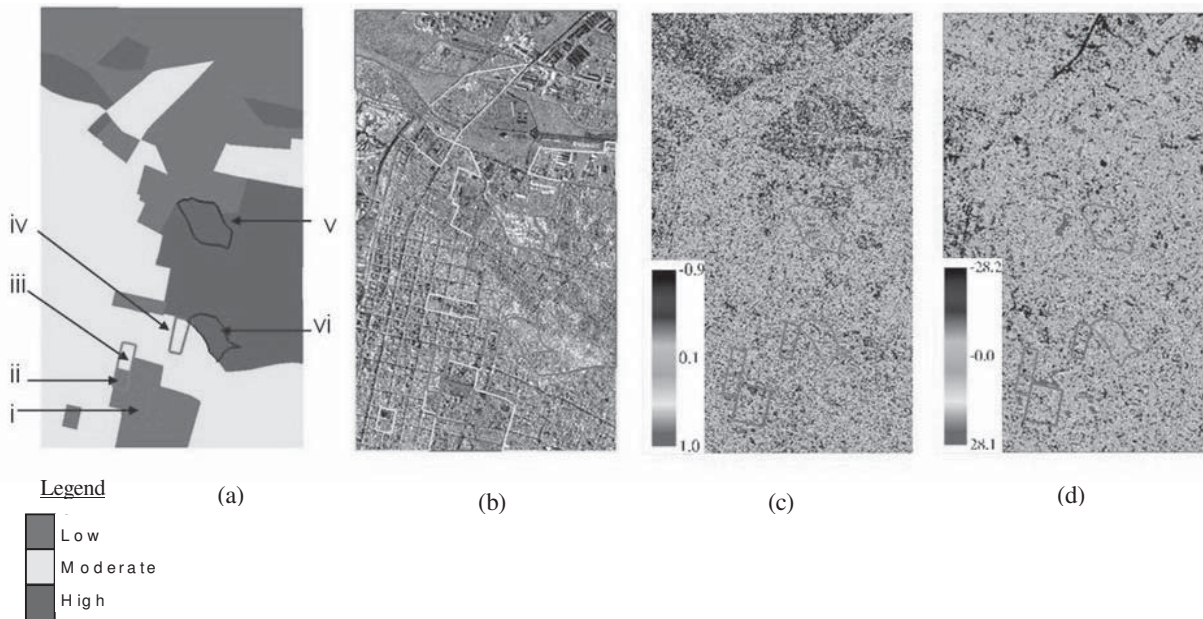


Figure 6 (a) Urban density of study area. Sampled areas in each density class are marked from (i) to (iv) (b) Color composite (Red: post-event, Cyan: pre-event) (c) Correlation map (d) Backscattering map

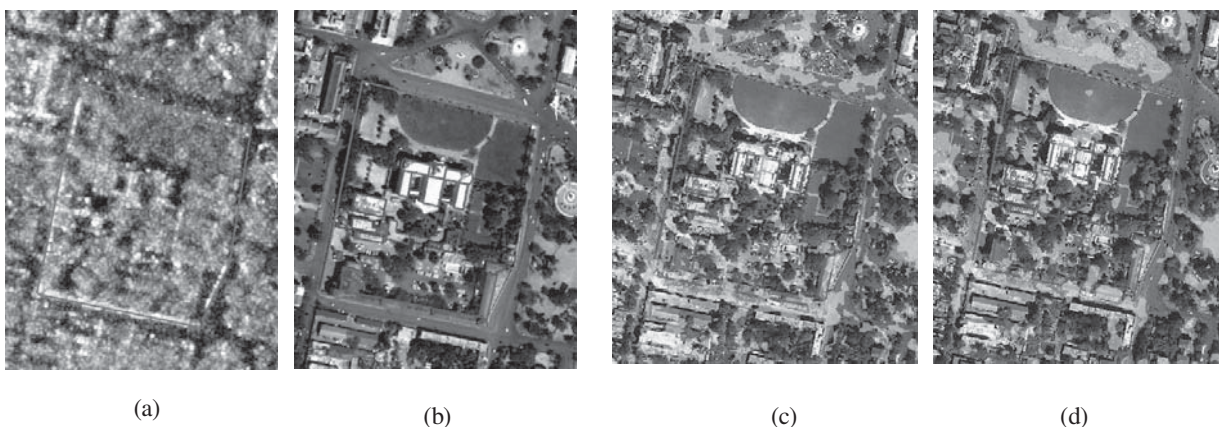


Figure 7 Example of low density area (sample area i in Figure 6(a)). (a) Color composite (Red: post-event, Cyan: pre-event) (b) Pre-event QuickBird image (c) Post-event GeoEye image with damaged buildings in red color polygons and subsequent overlay of low correlation, $r \leq 0.25$ and low NDVI (≤ 0.1) (d) Overlay of high backscatter difference, $d \leq -4$ dB & $d \geq 4$ dB: yellow color shows the high negative d while orange color is the high d

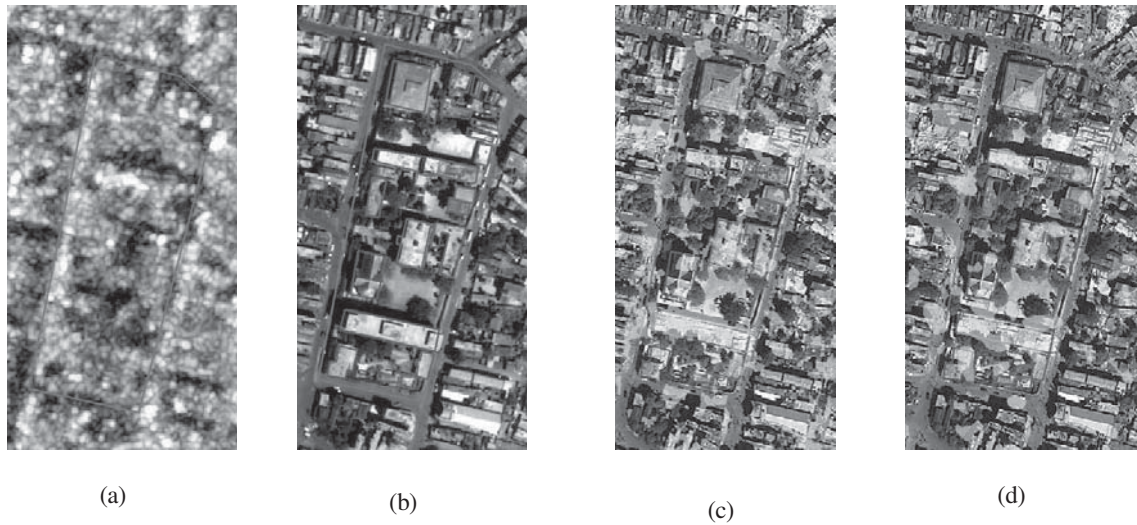


Figure 8 Example of moderate density area (sample area iv in Figure 6(a)). (a) Color composite (Red: post-event, Cyan: pre-event), (b) Pre-event QuickBird image (c) Post-event GeoEye image with damaged buildings in red color polygons and subsequent overlay of low correlation, $r \leq 0.25$ and low NDVI (≤ 0.1) (d) Overlay of high backscatter difference, $d \leq -4$ dB & $d \geq 4$ dB: yellow color shows the high negative d while orange color is the high d

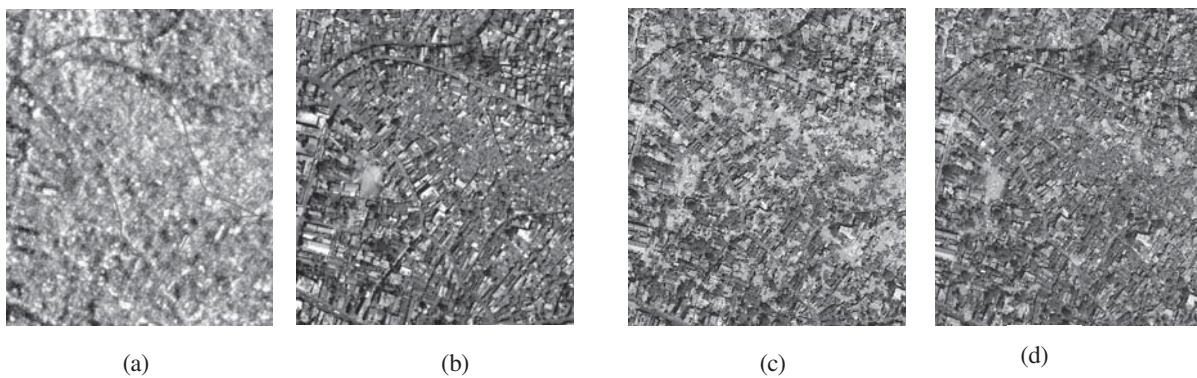


Figure 9 Example of high density area (sample area vi in Figure 6(a)). (a) Color composite (Red: post-event, Cyan: pre-event), (b) Pre-event QuickBird image (c) Post-event GeoEye image and subsequent overlay of low correlation, $r \leq 0.15$ and low NDVI (≤ 0.1) (d) Overlay of high backscatter difference, $d \leq -4$ dB & $d \geq 4$ dB: yellow color shows the high negative d while orange color is the high d

Table 1 Error matrix for low- and moderate-density areas

| | Damage | No damage | Sum | User's accuracy (%) |
|-------------------------|-----------|-----------|------------|---------------------|
| Damage (G5,G4) | 50 | 26 | 76 | 65.8 |
| No damage (G3,G2,G1) | 28 | 60 | 88 | 61.2 |
| Sum_PDNA | 78 | 86 | 164 | |
| Producer's accuracy (%) | 64.1 | 69.8 | | |
| Overall accuracy (%) | | | | 67.1 |

Regarding the high density areas as in the Figure 9, the total area covered by of low correlation ($r \leq 0.15$) and high backscatter difference ($d \leq -4$ dB & $d \geq 4$ dB) in two sampled blocks is 31, 693.79 m² while the blocks have area of 150, 290.05 m². So the possible damage area is about 21%. The reason of low detection ratios from SAR imagery might be explained by the density of the study area. It is to be mentioned that although we used PDNA's result as the truth data, it was produced from the visual inspection of satellite and vertical aerial images. Therefore, survey data from the ground is necessary for the more detailed evaluation.

4. CONCLUSIONS

We use the high-resolution TerraSAR-X images for detecting the building damages for the 2010 Haiti Earthquake. Backscatter characteristics like correlation coefficient (r) and backscatter difference (d) were calculated from pre- and post-event intensity images. Building damage detection was evaluated for three different density areas using the threshold values of r and d . Damaged buildings were effectively detected with low correlation coefficient and high backscatter differences. The results from analysis show effectiveness of the high-resolution SAR images in detecting the building damage even in the densely populated areas such as Port-au-Prince.

Acknowledgements:

The TerraSAR-X images used in this study were made available from SAR Application Research Committee, organized by PASCO Corporation, Tokyo, Japan.

References:

- Breit, H., Fritz, T., Balss, U., Lachaise, M., Niedermeier, A., and Vonavka, M. (2010), "TerraSAR-X SAR Processing and Product", *IEEE Transaction on Geoscience and Remote Sensing*, 48 (2), 727-740
- Eberhard, M.O., Baldrige, Steven., Marshall, Justin., Mooney, Walter., and Rix, G. J. (2010), "The MW 7.0 Haiti Earthquake of January 12, 2010; USGS/EERI Advance Reconnaissance Team Report: U.S. Geological Survey Open-File Report 2010-1048", 58.
- Infoterra. (2008), "Radiometric Calibration of TerraSAR-X data".
- ISDR. (2010), <http://www.unisdr.org/eng/library/lib-terminology-eng%20home.htm>.
- Lee, J. S. (1980), "Digital Image Enhancement and Noise Filtering by Use of Local Statistics", *IEEE Transaction, Pattern Analysis and Machine Intelligence*, *Photographic Surveying and Remote Sensing*, Vol.2, No.2, 165-168.
- Government of Haiti. (2010), Action Plan For National Recovery and Development of Haiti
- Matsuoka, M., and Yamazaki, F. (2004), "Use of Satellite SAR Intensity Imagery for Detecting Building Areas Damaged due to Earthquakes", *Earthquake Spectra*, 20 (3), 975-994.
- Matsuoka, M., and Yamazaki, F. (2005), "Building Damage Mapping for the 2004 Nigata-ken Chetsu Earthquake using Radarsat Images", *Earthquake Spectra*, Vol.21 (SI), 285-294.
- Matsuoka, M., Yamazaki, F., and Ohkura, H. (2007), "Damage Mapping for the 2004 Nigata-ken Chetsu Earthquake using Radarsat Images", *Urban Remote Sensing Joint Event*, IEEE, Paris, France, CD-ROM.
- Matsuoka, M., and Yamazaki, F. (2010), "Comparative Analysis For Detecting Areas With Building Damage from Several Destructive Earthquakes using Satellite Synthetic Aperture Radar Images", *Journal of Applied Remote Sensing*, SPIE, 4 (1), 1-16.
- Reliefweb. (2012), http://www.reliefweb.int/sites/reliefweb.int/files/resources/Full_Report_3325.pdf
- Stramondo, S., Bignami, C., Chini, M., Pierdicca, N., and Tertulliani, A. (2006), "Satellite Radar and Optical Remote Sensing for Earthquake Damage Detection: Results for Different Case Studies", *International Journal of Remote Sensing*, 27 (20), 4433-4447.
- Thao, N.V., Lan, D. T., Huong D.T., and Ve, N.D. (2010), "Assessing Damage of Flood by using ALOS Data in Thua Thien-Hue Province", *The 4th Joint PI symposium of ALOS Data nodes for ALOS Science Program*, Tokyo, Japan, 125.
- Time. (2012), <http://www.time.com/time/world/article/0,8599,2041450,00.htm#ixzz1jspmAwn>
- United Nations Institute for Training and Research (UNITAR), Operational Satellite Applications Programme (UNOSAT) European Commission (EC), Joint Research Centre (JRC) and The World Bank. (2010), "Atlas of Building Damage Assessment Haiti earthquake 12 January 2010 in support to Post Disaster Needs Assessment and Recovery Framework (PDNA)."
- United Nations Development Programme. (2010), <http://www.ht.undp.org/?lang=en&PHPSESSID=c3a4637485efbb3623ee7dca511280b3>
- Yonezawa, C. and Takeuchi, S. (2001), "Decorrelation of SAR data by Urban Damages Caused by the 1995 Hyogoken-nanbu Earthquake," *International Journal of Remote Sensing*, Vol.22 No.3, 1585-1600.